IEEE Access
Multidisciplinary ⋮ Rapid Review ⋮ Open Access Journal

Received January 22, 2022, accepted February 4, 2022, date of publication February 15, 2022, date of current version February 24, 2022.

Digital Object Identifier 10.1109/ACCESS.2022.3151849

High-Q High Power Tunable Filters Manufactured With Injection Molding Technology

MICHAEL D. SINANIS[1,2], (Student Member, IEEE), PINTU ADHIKARI[2], (Member, IEEE), THOMAS R. JONES[2,3], (Member, IEEE), MAHMOUD ABDELFATTAH[4], (Member, IEEE), AND DIMITRIOS PEROULIS[2], (Fellow, IEEE)

[1]School of Industrial Engineering, Purdue University, West Lafayette, IN 47907, USA
[2]Elmore Family School of Electrical and Computer Engineering, Purdue University, West Lafayette, IN 47907, USA
[3]Department of Electrical and Computer Engineering, University of Alberta, Edmonton, AB T6G 1H9, Canada
[4]Skyworks Solutions Inc., Newbury Park, CA 91320, USA

Corresponding author: Michael D. Sinanis (msinani@purdue.edu)

ABSTRACT This paper presents the first demonstration of injection molding technology to enable large-scale mass manufacturing of high-performance tunable microwave filters to meet the growing needs of 5G small cell stations. This is the first time that a tunable filter satisfies all four of the following requirements simultaneously: low manufacturing cost, high quality factor, wide tuning range, and high power handling. Exhaustive research exists on the use of polymers for 3D microwave device manufacturing; nonetheless, mass-production technologies, such as injection molding, can provide low costs without compromising performance. The proposed bandpass filter implementation uses a tunable evanescent-mode cavity resonator injection molded with an acrylonitrile-butadiene-styrene thermoplastic polymer. In addition, changing the critical gap size over the resonator's post using a commercial microactuator provides frequency tuning. The measured filter achieves an 86% tuning range from 2.8 – 5.2 GHz with a state-of-the-art measured unloaded quality factor Q_u of 1548 – 2573. The filter has a measured insertion loss of 0.06 - 0.1 dB with a fractional bandwidth from 7.6 - 8.4% across the entire tuning range. Moreover, for the first time in this manufacturing technology implementation, a bandpass filter is demonstrated with power handling capabilities beyond 100 W. The manufactured device demonstrates the significant potential of this technology for the scale-up manufacturing of reconfigurable high-Q RF filters without compromising the performance.

INDEX TERMS Evanescent-mode cavity filter, quality factor (Q), reconfigurable filter, tunable filter, injection molding, scale-up manufacturing method.

I. INTRODUCTION

The roll-out of 5th generation (5G) wireless communication technology is constantly demanding the increase of available communication bands. The next generation of factory equipment, vehicles, and personal devices will generate and transmit massive amounts of data in real-time. These 5G communication networks require a significant increase in the available channels. The challenge lies in the coexistence of all these channels without interference between them. Currently, more than 50 frequency bands are used in 4G networks, and it is expected that they will increase to 75 or 100 as more advanced 5G networks are rolled out globally, thereby expanding the complexity of the RF front-end [1]. Moreover, a 100X increase in the network at the edge through the introduction of small cell towers exponentially increases hardware costs and requires a higher degree of self-configuration. A recent report [2] estimates that 45 million 5G small cell towers would be installed by the end of 2031. Reconfigurable filters offer an alternative solution to lower costs and increase the performance of small cell station.

Evanescent-mode (EVA) resonators are capable of delivering high-performance devices [3]–[13]. Most recently, efforts have been focused on minimizing manufacturing costs while preserving performance. Hickle [14] has shown promising results with printed circuit board (PCB) manufacturing, demonstrating wide tunability of 91% tuning range, from 3.2–6.1 GHz. Simultaneously, this manufacturing method is in line with the current manufacturing method of millimeter-wave components for cost reduction. Research

The associate editor coordinating the review of this manuscript and approving it for publication was Rajeeb Dey.

has also been advancing for EVA-mode devices to match the demand of 5G for higher frequencies by pushing the PCB manufacturing boundaries. In [15] a high frequency band-stop filter is shown tuning from 22–42 GHz with state-of-the-art performance with less than 1 dB out-of-band insertion loss. Advancements in well-established technologies, such as injection molding (IM), are candidates for lower cost, high performance, scalable manufacturing, and great potential to deliver on these research efforts.

The main objective of this work is to demonstrate low-cost and high-performance through manufacturing with IM technology of an air-filled EVA-mode resonator and its implementation in a second-order bandpass filter (BPF). An unloaded quality factor (Q_u) ranging from 1548-2573 was measured, representing state-of-the-art performance and a record power-handling of more than 100 W. The content of this paper is organized as follows. Section II introduces the IM technology and the design considerations for this manufacturing method. Section III presents the resonator and the filter RF designs. Section IV presents the manufactured devices and their measured performance. Power handling was also investigated. Finally, Section V presents comparisons with state-of-the-art and discusses the results.

II. DEVICE ARCHITECTURE AND MANUFACTURING TECHNOLOGY

In recent years, much interest has been shown to generate high-performance devices for wireless communications through new technologies such as additive manufacturing [16]. In [3] state-of-the-art performance is demonstrated with a measured Q_u between 1638 and 3520 on a novel monolithic air-cavity bandpass filter using additive manufacturing. Simultaneously, 3D printing technologies continue to generate better results as the industry delivers machines that can match higher standards in geometrical tolerances and expand into new materials with a broad portfolio of properties. Emphasis has been placed on their performance while maintaining a low manufacturing cost, from design to end product.

IM of thermoplastics is used widely on everyday-use products. In recent years, micro-IM technology has advanced to deliver parts with tight tolerances on the order of microns. These can be successfully metalized with finely finished surfaces while producing parts with complex 3D geometries, providing a significantly lower cost per part and lower weight per volume, with the same or better characteristics of a machined part. Moreover, micro-IMs have the potential to generate components for higher frequency bands as well, as they can maintain the required micrometer-scale tolerances.

A. DEVICE CONCEPT

The conceptual structure of a tunable EVA-mode air-filled cavity resonator, which was considered during the design process for the IM, is shown in Fig. 1. Tunable EVA-mode cavity resonators have two essential parts: (a) a static cavity with a post located in the center, and (b) a flexible ceiling that serves as a tuning element. The walls of the air-filled cavity must be formed using conductive metal. To realize such a cavity, it is necessary that it be manufactured in two parts and assembled at a later step. Moreover, the tuning element requires a method of actuation that has been previously demonstrated using electrostatic [17], magneto-static [4], and piezo-static [6] technologies. Because our goal is to demonstrate the technology related to device performance, actuation is performed using a commercially available submicron linear positioner. The positioner's cost is not taken into consideration, given that it can be chosen in accordance with the desired application. Finally, one crucial structural parameter is the bonding of the two parts to create an air cavity. Different methods have been demonstrated using mechanical pressure, conductive epoxy [7], and thermo-compression bonding, as reported in [17]. In this work, we incorporated a mechanical bonding technique for simplicity.

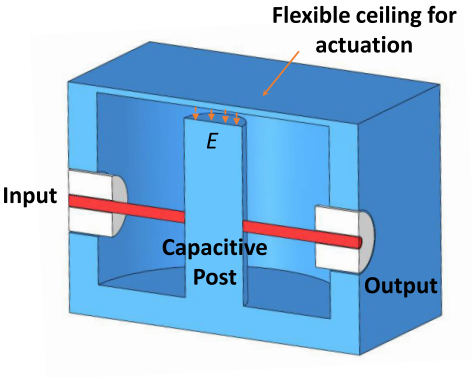

FIGURE 1. Conceptual structure of an EVA-mode air-filled cavity resonator.

Technological limitations and capabilities were considered to define the best possible design for part manufacturing, part assembly, and device performance. One critical parameter is the flexible upper wall of the air-filled cavity, which serves as a tuning element. An external actuator facilitates its accurate movement to control the resonant frequency of the device. As such, the large diameter of the tuning membrane allows for more deflection, which dictates the resonator tuning range. The geometrical characteristics, such as the diameter of the post, the diameter of the cavity, depth of the cavity, and actuation length of the membrane, will be modified in the RF design and will be analytically explained in Section III.

B. INJECTION MOLDING TECHNOLOGY

IM technology is widely used to produce products we use in our everyday lives by injecting molten thermoplastic into a mold. It is the most commonly used mass manufacturing process, capable of providing competitive characteristics for the manufactured parts, such as surface finish, tolerance, and geometrical structures compared to other manufacturing methods. Moreover, it offers the capability of mass-producing parts at the lowest cost and fastest production time.

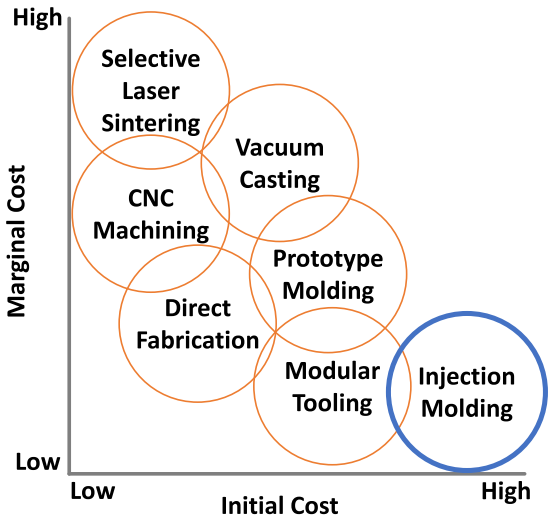

FIGURE 2. Manufacturing cost comparison of plastic technologies [18].

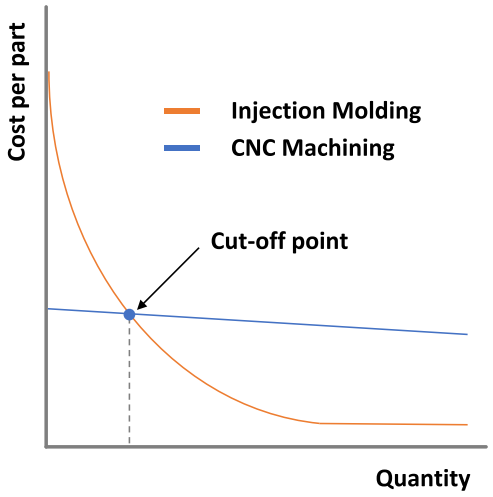

FIGURE 3. Cost cut-off point in comparison between IM and CNC machining.

The analysis conducted by Karania and Kazmer [18] clearly shows the advantage of IM compared to sister technologies when large-scale manufacturing is taken into consideration. Despite having a high initial setup cost, it is the most competitive when the marginal cost and production time are considered, as shown in Fig. 2 [18]. Their results for a non-complex experimental part showed that conventional injection molding is most suitable for quantities above 10,000 parts. As shown in Fig. 3, there is a cut-off amount beyond which the IM cost per part is significantly lower than that of other traditional technologies, such as CNC machining. Moreover, IM can deliver parts that maintain precision in the order of microns [19], surface finish, and structural strength. Table 1 highlights the advantages of the IM technology compared to other traditional manufacturing methods available for fast production. It should be noted that high-Q resonators manufactured using PCB technology require drilling via holes realized using a high-speed CNC machine, placing them in the CNC milling category.

TABLE 1. Additive manufacturing technology comparison [18].

	Resin Availability	Surface Finish	Part Integrity	Part Complexity
Conventional IM	↑↑↑	↑↑↑	↑↑↑	↑
Fused Deposition Modeling (FDM)	↓↓	↓↓	↓	↑↑↑
Selective Laser Sintering (SLS)	↓↓	↓↓	↓	↑↑↑
CNC Machining (China)	↑↑	↑↑	↑↑	↑

C. MATERIAL SELECTION

The broad utilization of plastics to produce end-use parts and products has led to the development of polymers as critical materials in modern manufacturing. There is a versatile category of materials with thousands of polymer options and properties for use. In some applications, thermoplastics are direct substitutes for metal parts delivering reduced weight and cost without compromising the performance [20]. In contrast to thermosets, thermoplastics can go through numerous melt and solidification cycles without significant degradation allowing for maximum product utilization, minimizing overall production costs.

Acrylonitrile butadiene styrene (ABS) is one of the most common plastics used in IM manufacturing. It has the valuable property of not burning. It rather liquefies upon reaching its melting point, which makes it ideal for IM applications. Simultaneously, it is possible to cool and reheat it without significant degradation. This characteristic provides a cost-effective option, as it reduces manufacturing waste. It is a tough, versatile, engineering thermoplastic that combines strength and durability with good heat resistance. Moreover, ABS is one of the best options for plating on plastic because of its chemical resistance characteristics. Adherent metal finishing can be deposited through chemical pretreatment and further metalized without compromising the structural and surface characteristics. In contrast, this metal layer enhances material attributes related to strength and heat resistance, a vital aspect to consider in high power applications, where the generated heat is a critical parameter impacting performance. The general material properties of ABS are listed in Table 2 [21].

D. DESIGN FOR MOLDABILITY

There are three main principles that one must abide by when designing a structure that will be injection molded: (1) undercuts, (2) uniformity, and (3) drafts [22]. The mold was composed of two parts: a cavity and a core. When they come together, their enclosure forms the cavity to be filled by the molten thermoplastic, and their contact forms the parting line. They were machined with high precision in order to

TABLE 2. ABS general material properties.

Physical Properties	ASTM Test Method	Units	Nominal Value
Density	D1505	g/cc	1.03
Tensile Strength @Yield	D638	psi	>6,000
Elongation @Break	D638	%	40
Flexural Modulus	D790	psi	300,000
Flexural Yield Strength	D790	psi	10,700
Durometer	D785	R scale	102
Izod Impact	D256	ft lbs/in^2	7.7
Vicat Softening Temp.	D1525	°F	219
Heat Deflection Temp. 66 psi	D648	°F	201
Flammability	UL94	UL94	HB

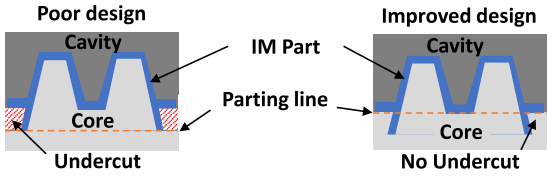

FIGURE 4. Parting line location for the mold. Poor design vs. Improved design.

FIGURE 5. Wall uniformity considerations for the mold. Poor design vs. Improved design.

guarantee a tight fit enclosure. Complex molds require slides or handloaded cores to form intricate shapes. This increase the complexity of the mold and, in rugged designs, the limit at which the parting line of the mold is located. Fig. 4 shows the parting line located in the proposed design and how it can be modified to simplify the design of the mold and guarantee a successful injection molded part.

Uniformity refers to the wall thickness of the IM plastic part. It should be the same across it in order to maintain cosmetic and structural integrity. A sink occurs when a thicker area of a part cools at a different rate, pulling faces towards its center. As depicted in Fig. 5, a poor design results in sinking marks that can be avoided by modifying it to have a wall of uniform thickness.

The draft angles are necessary for the part to be released from the mold. A deep cavity increases the length of the pull, and a lack of draft causes drag marks or scratches on the sides of the part. In this design (Fig. 6), a small draft of 15° is recommended to allow for a more accessible release of the part.

Geometrical characteristics are essential in the design of EVA devices and have been considered in the construction of resonators and second-order BPFs. Any possible undercuts were eliminated, and the part was designed to have a uniform

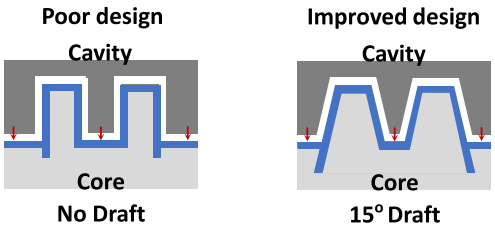

FIGURE 6. Draft angle considerations for the mold. Poor design vs. Improved design.

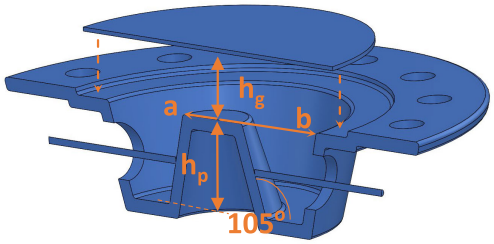

FIGURE 7. Proposed injection molded cavity resonator.

thickness of 1 mm. The drafted sidewalls of the cavity were designed ten times the available lower limit at 15° to obtain the necessary high surface finish.

III. RESONATOR AND FILTER RF DESIGN

A. RESONATOR

Fig. 7 presents a 3-D view of the proposed IM cavity resonator and shows three critical dimensions and geometry for design optimization: (1) the RF gap (h_g), which is modulated to create the frequency tuning between the flexible membrane and the center post; (2) the height of the post (h_p); and (3) the 105° angled walls, which are critical for maintaining smooth surface roughness during the IM process. The tuning element on top of the post-loaded cavity resonator was implemented using a liquid crystal polymer (LCP) membrane metalized with copper on one side (Ultralam 3850 by Rogers Corp.). A commercial linear actuator (M3L-S by New Scale Technologies), moves the membrane by changing the gap (h_g) vertically. Based on the dimensions of the EVA-mode air-filled cavity summarized in Table 3, its resonance frequency (f_0) can be calculated using the following equation [8]:

$$f_0 = \frac{1}{2\pi\sqrt{L_{cav}C_{eqv}}} \tag{1}$$

where cavity inductance (L_{cav}) is given below:

$$L_{cav} = \frac{1}{6\pi \times 10^8}\sqrt{\frac{\mu_0}{\epsilon_0}}ln(\frac{b}{a})\,h_p. \tag{2}$$

C_{eqv} is the total approximate capacitance between the post and membrane C_{pm} and the post and the cavity C_{pc}, and can be calculated using the following equations [8]:

$$C_{eqv} = C_{pm} + C_{pc} \tag{3}$$

$$C_{pm} \approx \frac{\epsilon_0\pi a^2}{h_g} \tag{4}$$

TABLE 3. Designed EVA-cavity resonator parameters.

Parameter	Value
Post radius, a	3.0 mm
Gap (min-max), h_g	45.7 - 540 μm
Post height, h_p	6.8 mm
Cavity radius, b	10.0 mm

$$C_{pc} \approx \frac{2\pi}{6 \times 10^8 \sqrt{\frac{\mu_0}{\epsilon_0}} ln(\frac{b}{a})} h_p. \quad (5)$$

The other essential parameters of the IM cavity resonator are described as follows. The frequency tuning of the resonator depends primarily on C_{pm}. A change in the gap height h_g between the post and the membrane changes C_{pm}, thus changing the resonant frequency and tuning the resonator. In this particular resonator design, the lowest gap considered is 45.7 μm, which corresponds to the lowest resonance frequency of 2.0 GHz, and the highest gap is 540 μm, which corresponds to the highest resonance frequency of 5.0 GHz.

Q_u and the analytical equation of Q_u for a traditional EVA-mode cavity resonator were derived in [15]. Q_u is the most crucial parameter of a resonator circuit and indicates the loss associated with the resonator (a lower loss implies a higher Q_u). In general, resonators suffer losses due to conductor loss, dielectric loss, and radiation loss. With an air-filled cavity, the IM resonator had the lowest possible dielectric loss. Radiation loss is also low because of the close contact between the flexible ceiling and cavity. To minimize conductor loss, the IM technology implementation aimed at a high surface finish for the part, which was maintained during metalization by utilizing a reverse power plating (RPP) method ($R_a = 0.31$ μm) [23].

B. FILTER

A two-pole reconfigurable BPF utilizing the EVA-mode cavity resonator was designed using standard coupling synthesis techniques to demonstrate the proposed manufacturing method and validate its performance. The design procedure for tunable EVA-mode cavity filters has been extensively reported in the literature [8], [9], [24], thus only a brief discussion is included here. A 3-D sketch of the filter is shown in Fig. 8 with final design dimensions summarized in Table 4. The flexible membrane that encloses the cavity serves as the tuning element. A section cut of the device shows the internal structure of the cavity and its design parameters.

The filter response type and fractional bandwidth (FBW) depend on the cavities' external input/output and inter-resonator couplings. The external couplings are evaluated by the external quality factor Q_e, and the inter-resonator coupling k_{12} is evaluated by the even-mode (f_m) and odd-mode (f_e) resonance frequencies of a coupled-resonator system [25]. For this particular design, a Chebyshev BPF response at 2.8 GHz ($h_g = 101$ μm) with 7.6% FBW and 30 dB minimum return loss is initially designed, with

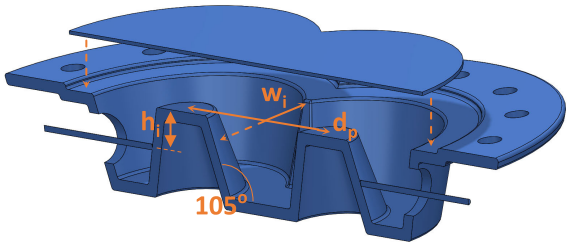

FIGURE 8. Proposed injection molded cavity filter.

TABLE 4. Designed EVA-cavity filter parameters.

Parameter	Value
Post radius, a	3.0 mm
Gap (min-max), h_g	101 - 588 μm
Post height, h_p	6.8 mm
RF input height, h_i	3.5 mm
Cavity radius, b	10.0 mm
Post distance, d_p	16.0 mm
Iris width, w_i	13.0 mm

calculated coupling values $Q_e = 4.76$, and $k_{12} = 0.22$. A highly coupled response is chosen to achieve low insertion loss in the passband.

The required external coupling was realized by an RF connector inserted through the sidewall of the cavity and short circuited on the metalized sidewall of the capacitive post. The coupling strength is controlled by the distance of the pin from the top of the post, as shown by dimension h_i in Fig. 8. The closer the pin is to the top of the post (smaller h_i), the stronger the external coupling becomes. Ensuring that the tip of the pin makes good contact with the sidewall of the post is also important. If the contact between the pin and the post is poor, the coupling is reduced. To determine the dimension h_i, a single EVA-mode cavity resonator fed by an RF connector is simulated in HFSS, and the required Q_e for a given h_i is extracted from S_{11} using the group delay method, where $Q_e = 2\pi f_0 \tau(f_0)/4$, and $\tau(f_0)$ is the reflection group delay at resonance [26]. For this design, the pin was located 3.5 mm below the top of the post to achieve the desired Q_e.

The iris located between the two resonators implements the necessary inter-resonator coupling, where the dimensions W_i and d_p shown in Fig. 8, along with the overall shape of the iris, determine the coupling strength [8]. The closer the two posts are together (smaller d_p), or the wider the iris opening (larger W_i), the stronger the coupling. To determine the dimensions W_i and d_p, two iris coupled EVA-mode cavity resonators without RF connectors are simulated in the eigen-mode solver of the HFSS. For a given set of dimensions W_i and d_p, the even- and odd-mode resonance frequencies were extracted and the coupling coefficient was calculated using $k_{12} = (f_e^2 - f_m^2)/(f_e^2 + f_m^2)$ [25]. The iris dimensions providing the desired k_{12} were determined to be $W_i = 13$ mm and $d_p = 16$ mm. It should be noted that a more comprehensive design procedure for tunable EVA-mode cavity BPFs was

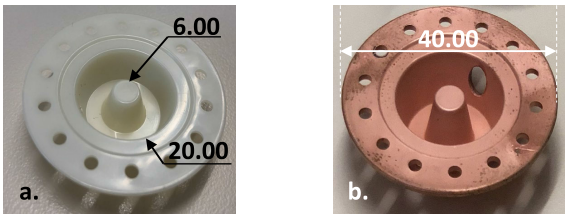

FIGURE 9. ABS injection molded cavity resonator. a. molded cavity, b. copper electroplated cavity.

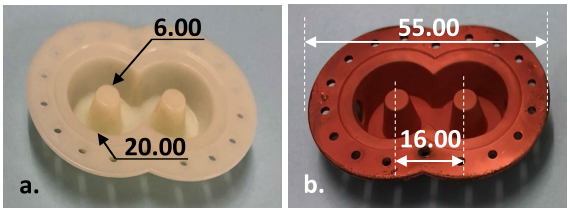

FIGURE 10. ABS injection molded cavity filter. a. molded cavity, b. copper electroplated cavity.

reported in [8], with considerations for a constant bandwidth or constant FBW across the entire tuning range. Although not implemented here, the proposed structure allows for such improved performance features.

Finally, a flexible membrane is used to enclose the cavity top to provide vertical movement and control the air gap (h_g) to tune the filter. An LCP layer was mechanically pressed against the sidewalls to achieve good contact, thus maintaining a high Q_u. Two external microactuators individually control the two separate tuners, changing h_g from 101 μm to 588 μm, thus tuning the filter from 2.8 to 5.2 GHz.

IV. FABRICATION AND MEASUREMENTS

A. RESONATOR

A cavity core was manufactured in aluminum through precision CNC machining and used in industrial level IM equipment by Proto Labs Inc. During the manufacturing process, molten ABS material was injected through the mold, and the part was released at the end of the cycle. The produced cavity parts are shown in Fig. 9 and Fig. 10, for the resonator and BPF, respectively. The manufactured parts were solvent cleaned, and the surface was prepared for metalization. Initially, the surface was treated with an Argon plasma for 60 seconds in a desktop reactive ion etcher (RIE) to increase the adhesion of the seed metal. Next, the samples were inserted in a magnetron sputtering equipment to deposit a total of 0.5 μm seed layer of Ti/Au (20 nm of Ti) to electroplate a thick copper layer. The samples were placed in a copper sulfate bath, and an RPP method was used to obtain a high density and fine surface finish [23]. The LCP membrane used as a tuning element was 25 μm thick and metalized with a 9 μm copper layer.

The final assembly also has a connector launch pad to facilitate the transition of the SMA connector inside the cavity. It has been CNC machined from bulk copper and serves as a pressure plate for the cavity and membrane seal. In addition, a CNC machined fixture was produced to align and hold the microactuators in position. The microactuator pillars were fixed on top of the tuning membrane using a conventional fast-drying adhesive layer. These fixtures can be eliminated from the final product by integration into one piece with the IM cavity. Images of the assembled devices are shown in Fig. 11 (a) and (b).

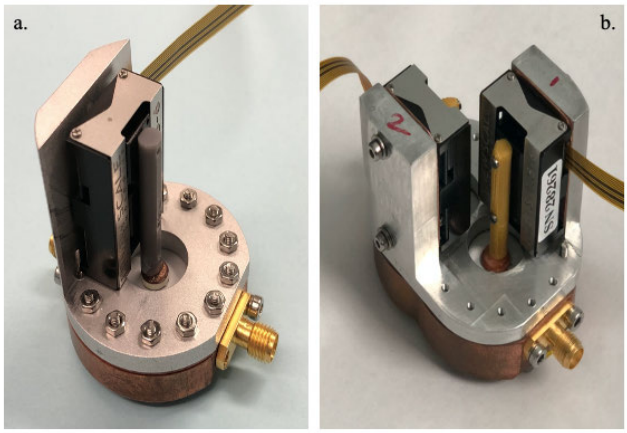

FIGURE 11. Assembled manufactured devices. a) resonator b) bandpass filter.

A weakly coupled EVA-mode cavity was manufactured to evaluate the Q_u of the tunable resonator. Referring to Fig. 7, the feeding pins were disconnected from the post to achieve weak coupling. The resonator was tuned to different gap heights by adjusting the position of the membrane above the post using a microactuator. Fig. 12(a) shows the measured results compared to simulation. The measured Q_u was extracted from the measured S_{21} for different tuning gap heights using the well known equation $Q_u = Q_L/(1 - S_{21}(f_0))$ [27], where Q_L is the loaded quality factor, and $S_{21}(f_0)$ is the measured insertion loss at resonance frequency f_0, as shown in Fig. 12(b). The simulated Q_u of the resonator was evaluated using the eigenmode solver in HFSS without including the effect of the connectors, likely accounting for the discrepancy seen between simulation and measurement, which includes SMA connector loss. Furthermore, the ideal bulk conductivity of copper ($\sigma = 5.8 \times 10^7$ S/m) given in HFSS was used for all simulations; in comparison the measured cavity suffers further losses due to copper surface roughness and other fabrication tolerances or assembly errors. The actual conductivity of the electroplated copper was not measured. The resonator was tuned from $2.0 - 5.0$ GHz using gap heights (h_g) of $45.7 - 520$ μm, respectively and achieved a measured Q_u of $1548 - 2573$.

B. FILTER PERFORMANCE MEASUREMENTS

In Fig. 13, the measured performance of the fabricated 2-pole IM EVA-mode cavity BPF designed in Section III.B

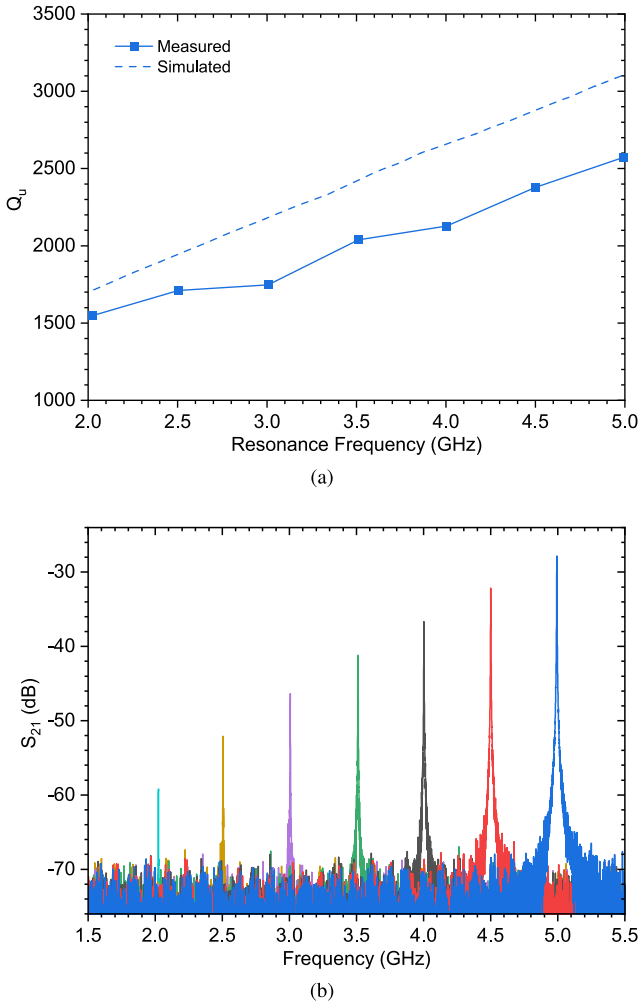

FIGURE 12. (a) Measured and simulated extracted Q_u of the weakly coupled single cavity resonator, and (b) measured insertion loss ($|S_{21}|$) of the weakly coupled single cavity resonator, with the colors representing different tuning gap heights (h_g) used to extract the measured Q_u at several resonance frequencies across the resonator's tuning range.

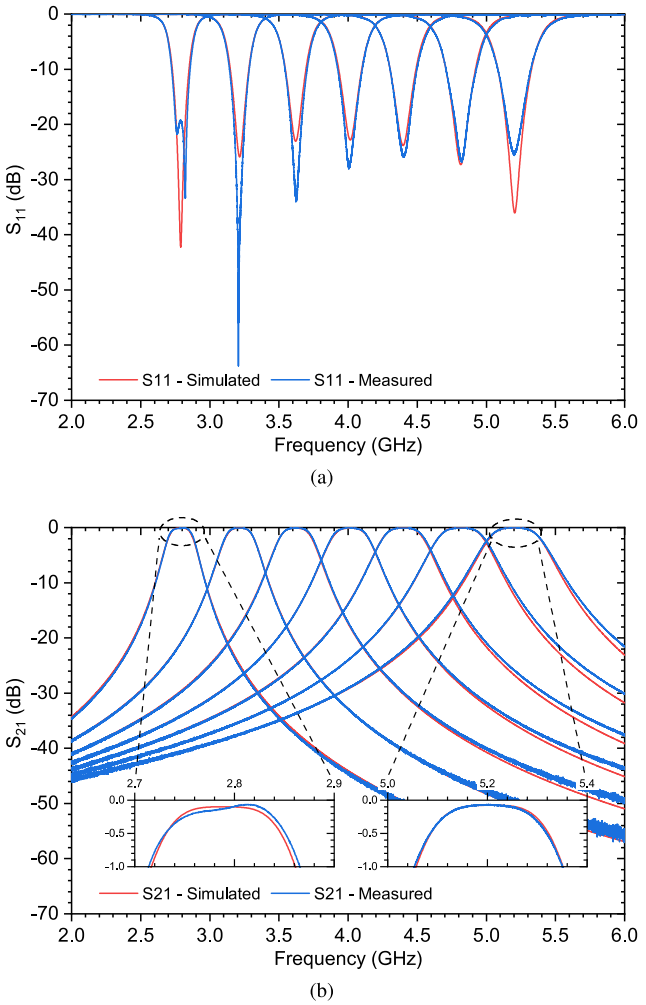

FIGURE 13. (a) Measured and simulated return loss ($|S_{11}|$) of the tunable cavity filter, and (b) measured and simulated insertion loss ($|S_{21}|$) of the filter, with insets showing a closer view of the in-band insertion loss for the lowest and highest bandpass filter responses (results include SMA connector loss).

is compared with the simulation results from the HFSS, with good agreement. Adjusting the simulated gap height from $101 - 588$ μm, the filter's center frequency is tuned from $2.8 - 5.2$ GHz, for a tuning range of 1.9:1. The return loss ($|S_{11}|$) of the fabricated device is shown in Fig. 13(a), with each tuning state achieving more than 20 dB matching. In Fig. 13(b) the insertion loss ($|S_{21}|$) of the filter is shown, with two insets giving a closer look at the in-band response for the lowest and highest bandpass frequencies. A copper conductivity of $\sigma = 5.8 \times 10^7$ S/m was again used in the simulation, along with the Teflon of the SMA connector with dielectric constant $\epsilon_r = 2.08$ and loss tangent $tan\delta = 0.001$ as given in the HFSS. The measured results include SMA connector loss. At a center frequency of 2.8 GHz, the measured filter has a minimum in-band insertion loss of 0.07 dB and a 3− dB FBW of 7.6%, while at a center frequency of 5.2 GHz, the measured filter has a minimum in-band insertion loss of 0.07 dB and an FBW of 8.4%. The minimum insertion loss across the entire tuning range varies between $0.06 - 0.1$ dB. A smoothing function on the measured data was used to remove measurement uncertainty of ± 0.01 dB when extracting the reported insertion loss values above.

C. POWER HANDLING

Power handling is a critical characteristic of high-performance cavity filters. Power handling of the EVA-mode cavities has been extensively investigated, and three main limitations have been identified: (1) tuning non-linearities, (2) self-heating, and (3) gas discharge [28]. Due to the significant RF tuning gaps implemented within the proposed design, the nonlinear behavior resulting from tuner self-actuation is not significant. Furthermore, this behavior depends not only on the RF gap but also on the tuning method of the resonator. This design uses an external microactuator with a 0.5 N holding force to maintain the tuner position and counteract the generated force.

EVA-mode cavities traditionally show good power handling capability due to their geometrical structure and

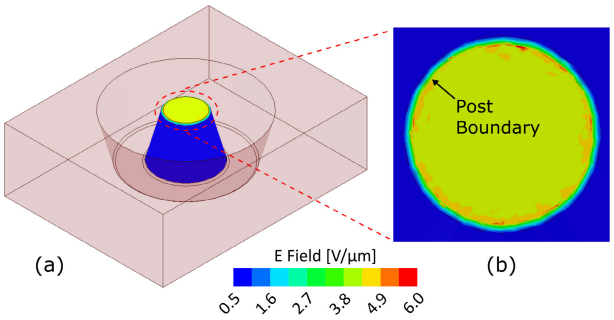

Air Gap h_g (μm)	$E_{max\text{-}norm}$ (V/μm)	$W_{stored\text{-}max}$ (nJ)	P_{max} (W/dBm)
43.1	0.65	3.51	41.9 / 46.2
48.1	0.60	3.10	55.9 / 47.5
92.8	0.35	1.96	260.4 / 54.2

FIGURE 14. (a) Simulated electric field distribution for air gap $h_g = 43$ μm on the post inside the cavity (tuner is not shown for better display), and (b) a closer view of the field strength on the top of the post, along with the calculated maximum power handling P_{max} for three different air gap sizes.

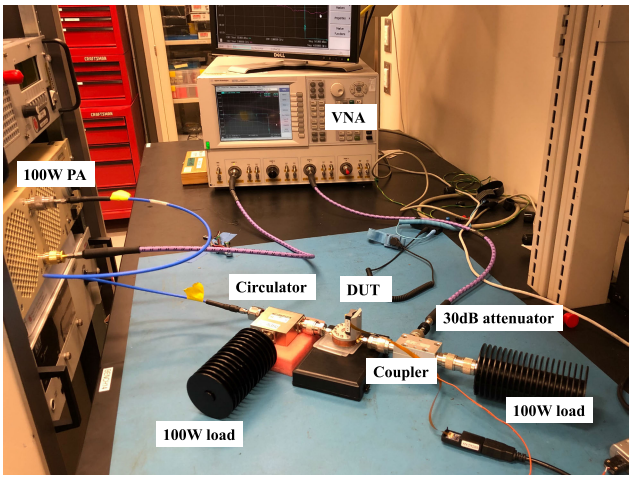

FIGURE 15. High power measurement setup.

significant gaps available during tuning. However, high power resonators designed to handle 100s of watts may fail because of gas breakdown [29]–[31]. Semnani *et al.* studied the gas breakdown and power handling of EVA-mode cavities and validated their theoritical and experimental findings [30]. It was shown that the main mechanisms of gas breakdown for relatively large air gaps (>10 μm) under atmospheric pressure were due to electron-induced ionization and secondary electron emission. In [32], a proposed method of predicting the maximum power handling of an EVA-mode cavity was investigated. The same method was used to predict the power handling capabilities of the IM EVA-mode cavity in this work before experimental validation.

For EVA-mode cavities, most of the electric field is concentrated within the small air gap between the top of the post and the tuner. Gas breakdown occurs when the electric field density in this region reaches a specific value. When this occurs, the resonator shorts, thus defining the maximum power handling of the device. The maximum power handling $P_{\max}$ of an EVA-mode cavity can be calculated from the following [32]:

$$P_{\max} = \left(\frac{E_{\text{breakdown}}}{E_{\max-\text{norm}}}\right)^2 \times \frac{1}{W_{\text{stored}-\max}} \tag{6}$$

where $E_{\text{breakdown}}$ is the electric field breakdown threshold of air, $E_{\max-\text{norm}}$ is the maximum magnitude of the simulated electric field inside the cavity using the eigenmode solver of HFSS normalized to 1 nJ, and $W_{\text{stored}-\max}$ is the maximum stored energy inside the cavity in nanojoules. For air gaps on the order of a few 10s of micrometers, $E_{\text{breakdown}}$ has been reported to be 7.9 V/μm [29].

The maximum stored energy inside the EVA-mode cavity can be calculated from:

$$W_{\text{stored}-\max} = \frac{1}{2} C_{eqv} V^2 \tag{7}$$

where C_{eqv} is calculated from (3). By exciting the simulated cavity in HFSS with 1 W of input power, the nodal voltage V across C_{eqv} can be extracted by multiplying the maximum magnitude of the electric field by the gap height.

In Fig. 14, the simulated electric field distribution on the post for an air gap $h_g = 43.1$ μm is shown, along with the calculations of $P_{\max}$ for three different air gaps. A close-up of the top of the post is also shown in Fig. 14(b), where it is clear that the majority of the field is located within this region. The calculated values for $P_{\max}$ were 41.9 W, 55.9 W, and 260.4 W for air gaps $h_g = 43.1$ μm, 48.1 μm, and 92.8 μm, and cavity resonance frequencies 2.0 GHz, 2.1 GHz, and 2.8 GHz, respectively.

The power handling of the manufactured resonator in section IV.A was investigated to compare the predicted power handling of the EVA-mode cavity with the measurement. A weakly coupled resonator reflects too much power and does not provide a good indication of the resonator's power handling. Thus, the amount of input/output coupling of the resonator was increased by adjusting the feed pin location to make contact with the post and achieve critical coupling. Fig. 15 shows the high power experimental setup. A single continuous wave (CW) power-swept stimulus from 33 dBm to 47 dBm was applied at the input of the resonator over a time period of 185 ms, with the forward transmission (S_{21}) versus input power measured at the resonance frequency of the cavity corresponding to a particular gap height. This measurement shows the breakdown power due to gas discharge by limiting the amount of time the resonator operates at a high power [29]. For longer measurement times, other high power effects became more prominent.

In Fig. 16, the measured power handling of the resonator is shown for two different gap heights. This height was estimated using the simulated model in the HFSS by correlating the measured frequency with the equivalent simulated gap. At a resonance frequency of 2.004 GHz, with an estimated gap height of 43 μm, no breakdown wass observed at a power-sweep time of 185 seconds up to 47 dBm. This indicates that the simulated power handling shown in Fig. 14 is a conservative estimation. Increasing the power-sweep

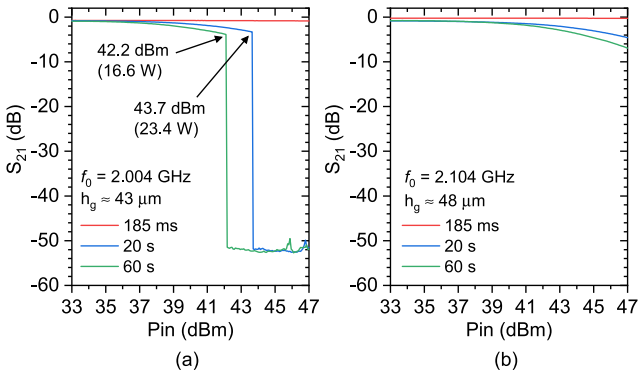

FIGURE 16. High power measurement results for the critically coupled cavity at (a) 2.0024 GHz and (b) 2.052 GHz.

TABLE 5. Comparison of this work with the state-of-the-art EVA-mode tunable cavity resonators.

Reference	Manufacturing and Tuning Technology	P_{max} (W)	Tuning Range (GHz)
[9]	PCB + Microactuator	>100	1.3 - 3.6
[10]	Machining + RF MEMS	0.004	4.07 - 5.58
[11]	PCB + Piezo Disk	10	2.2 - 2.8
[33]	3D Printing + Microactuator	-	1 - 3
[34]	Machining + Liquid Metal	-	2.9 - 9.9
This work	IM + Microactuator	>100	2 - 5

TABLE 6. Comparison of this work with the state-of-the-art EVA-mode cavity filters.

Reference	FBW (%)	IL (dB)	Tuning Range (GHz)	Quality Factor
[3]	13	0.35	5.2	3257
[12]	8.8	0.08	3.53	1833
[13]	8.4 - 9.1	0.77 - 0.26	2.2 - 4.2	500 - 700
[17]	-	3.14 - 0.78	18.9 - 39.6	265 - 510
[33]	4.1 - 8.5	<1.3	1.3 - 2.2	>500
[34]	-	<1	3.4 - 7.5	120 - 625
[35]	5.1	2.1	10.26	214
[36]	1.1	3.57 - 1.56	0.98 - 3.48	300 - 650
This work	7.6 - 8.4	0.06 - 0.1	2.8 - 5.2	1548 - 2573

time to 20 seconds, breakdown occurs at 43.7 dBm, and at 60 seconds, the breakdown occurs at 42.2 dBm. At a resonance frequency of 2.104 GHz, with an estimated gap height of 48 μm, breakdown did not occur at any measured sweep time. These results are discussed in the following Section V.

The method in [32] was also used to predict the power handling of the EVA-mode cavity BPF in Section IV.B, due to slight differences in the electric field distribution between the filter and resonator structures. The filter response at 2.8 GHz with a gap of 101 μm was evaluated because it had the narrowest FBW and smallest gap height, resulting in the worst-case scenario for power handling with the longest group delay and thus the largest amount of stored energy [37]. First, the maximum electric field magnitude for each individual resonator of the filter was extracted from the HFSS simulation model, noting that the peak field occurs at the edges of the passband and has a different magnitude for each resonator. By exciting the model with an input power of 1 W, the first resonator was found to have a greater field magnitude. From this value, the maximum stored energy, $W_{\text{stored}-\text{max}}$ was calculated using (7) and was found to be 2.32 nJ. Next, the filter was simulated using the eigenmode solver in HFSS normalized to 1 nJ, and the maximum normalized electric field $E_{\text{max}-\text{norm}}$ was extracted with a value of 0.33 V/μm. Using (6), the estimated power handling P_{max} of the EVA-mode cavity BPF was determined to be 244 W, or 53.9 dBm.

V. DISCUSSION

The high performance of the manufactured device for comparison purposes was defined by the unloaded quality factor Q_u and high-power handling capabilities. Both parameters were simulated, experimentally examined, and compared with the state-of-the-art. Tables 5 and 6 relate this work's manufactured resonator and filter, respectively, to state-of-the-art EVA-mode resonators and filters in the literature. The implementation of IM technology provides a high surface finish cavity, which is essential for a high-Q performance. In conjunction with applying a soft adhesive to ensure optimal contact of the flexible membrane, mechanical pressure bonding allows for superior electrical connections by eliminating the air gaps and radiation leakage, resulting in the best possible performance. The simplicity of the assembly minimizes manufacturing errors and produces measured results that are in good agreement with the simulated results.

Fig. 14 presents the simulated breakdown of the EVA-mode resonator based on different tuning gaps. These results are in good agreement with the measured results presented in Fig. 16(a) and (b). In addition, Fig. 14 shows the expected breakdown power of the resonator at 2.8 GHz (92.8 μm gap height), the lowest measured frequency response of the filter. The simulated breakdown of the EVA-mode BPF at 2.8 GHz was also determined, with only a slight decrease in power handling compared with the resonator. Thus, based on the designed and manufactured tunable filter's minimum gap of 101 μm, along with the good correlation between the single resonator's simulation and experimental results conducted at smaller gap heights, this indicates the filter's high-power handling (>100 W) capabilities within its tuning frequency range.

In summary, both manufactured devices showed outstanding performance compared to similar work. The resonator and filter differentiate from other works by exhibiting for the first time, a low insertion loss, wide tuning range, high power handling, and high-Q performance in the same working prototype. In Table 5, one can observe these trade-off characteristics in the realization of the state-of-the-art resonators. In [9] insertion loss was sacrificed for higher power handling, and in [34] the quality factor Q was sacrificed for a wider tuning range. In [12] a comparable insertion loss was shown but with a fixed frequency device. Finally, in Table 6 this

work exhibits simultaneously all three characteristics: insertion loss, tuning range, and quality factor Q, competitive with state-of-the-art filters.

VI. CONCLUSION

This work investigated the potential use of injection molding technology as a large scale low-cost manufacturing method to realize high-Q high power tunable filters. For demonstration, an injection molded tunable evanescent-mode cavity resonator and a bandpass filter were manufactured and tested. The measured filter achieved an insertion loss between $0.06 - 0.1$ dB within a tuning range from $2.8 - 5.2$ GHz, and an unloaded quality factor of $1548 - 2573$, comparable to existing state-of-the-art devices for a fraction of the cost per part produced. To demonstrate the power handling of the proposed technology, a strongly-coupled resonator was shown to handle high power loads at small gap heights, dictating the higher-order filter's capability to perform similarly. The presented results confirm the potential of this technology for the low-cost mass production of high-performance tunable filters in the sub-6 GHz range.

ACKNOWLEDGMENT

The authors would like to thank Zach Vander Missen for his advice with the power handling evaluation method and setup.

REFERENCES

[1] L. Getto, "The challenges of 5G network densification," *Microw. J.*, vol. 62, no. 5, p. 136, 2019.

[2] Y.-H. Chang. *45 Million of 5G Small Cells Will be Installed by 2031*. Accessed: Jun. 7, 2021. [Online]. Available: https://www.microwavejournal.com/articles/32235-the-challenges-of-5g-network-densification

[3] K. Zhao and D. Psychogiou, "Monolithic SLA-based capacitively-loaded high-Q coaxial resonators and bandpass filters," in *Proc. 50th Eur. Microw. Conf. (EuMC)*, Jan. 2021, pp. 471–474.

[4] M. S. Arif, W. Irshad, X. Liu, W. J. Chappell, and D. Peroulis, "A high-Q magnetostatically-tunable all-silicon evanescent cavity resonator," in *IEEE MTT-S Int. Microw. Symp. Dig.*, Dec. 2011, pp. 3–6.

[5] M. D. Hickle, M. D. Sinanis, and D. Peroulis, "Tunable high-isolation W-band bandstop filters," in *IEEE MTT-S Int. Microw. Symp. Dig.*, May 2015, pp. 1–4.

[6] E. J. Naglich, J. Lee, D. Peroulis, and W. J. Chappell, "High-Q tunable bandstop filters with adaptable bandwidth and pole allocation," in *IEEE MTT-S Int. Microw. Symp. Dig.*, Jun. 2011, pp. 1–4.

[7] E. J. Naglich, M. Sinani, S. Moon, and D. Peroulis, "High-Q MEMS-tunable W-band bandstop resonators," in *IEEE MTT-S Int. Microw. Symp. Dig.*, Oct. 2014, pp. 1–3.

[8] Z.-A. Yang, D. Psychogiou, and D. Peroulis, "Design and optimization of tunable silicon-integrated evanescent-mode bandpass filters," *IEEE Trans. Microw. Theory Techn.*, vol. 66, no. 4, pp. 1790–1803, Apr. 2018.

[9] M. Abdelfattah and D. Peroulis, "High-Q tunable evanescent-mode cavity siw resonators and filters with contactless tuners," *IEEE Trans. Microw. Theory Techn.*, vol. 67, no. 9, pp. 3661–3672, 2019.

[10] S.-J. Park, I. Reines, C. Patel, and G. M. Rebeiz, "High Q RF-MEMS 4–6-GHz tunable evanescent-mode cavity filter," *IEEE Trans. Microw. Theory Techn.*, vol. 58, no. 2, pp. 381–389, Jan. 2010.

[11] K. Chen, H. H. Sigmarsson, and D. Peroulis, "Power handling of high-Q evanescent-mode tunable filter with integrated piezoelectric actuators," in *IEEE MTT-S Int. Microw. Symp. Dig.*, Jun. 2012, pp. 1–3.

[12] K. Zhao and D. Psychogiou, "A monolithic vertical integration concept for compact coaxial-resonator-based bandpass filters using additive manufacturing," *IEEE Microw. Wireless Compon. Lett.*, vol. 31, no. 6, pp. 689–692, Jun. 2021.

[13] M. D. Sinanis, M. Abdelfattah, M. Cakmak, and D. Peroulis, "A 2.2–4.2 GHz low-loss tunable bandpass filter based on low cost manufacturing of ABS polymer," in *Proc. IEEE 19th Wireless Microw. Technol. Conf. (WAMICON)*, Apr. 2018, pp. 1–4.

[14] M. D. Hickle and D. Peroulis, "A widely-tunable substrate-integrated balun filter," in *IEEE MTT-S Int. Microw. Symp. Dig.*, Jun. 2017, pp. 274–277.

[15] P. Adhikari, W. Yang, Y.-C. Wu, and D. Peroulis, "A PCB technology-based 22–42-GHz quasi-absorptive bandstop filter," *IEEE Microw. Wireless Compon. Lett.*, vol. 28, no. 11, pp. 975–977, Nov. 2018.

[16] J. Sorocki, I. Piekarz, S. Gruszczynski, K. Wincza, and J. Papapolymerou, "Application of 3-D printing technology for the realization of high-performance directional couplers in suspended stripline technique," *IEEE Trans. Compon., Packag., Manuf. Technol.*, vol. 9, no. 8, pp. 1652–1658, Aug. 2019.

[17] Z. Yang, R. Zhang, and D. Peroulis, "Design and optimization of bidirectional tunable MEMS all-silicon evanescent-mode cavity filter," *IEEE Trans. Microw. Theory Techn.*, vol. 68, no. 6, pp. 2398–2408, Jun. 2020.

[18] R. Karania and D. Kazmer, "Low vol. plastic, manufacturing strategies," *ASME J. Mech. Des.*, vol. 129, no. 12, pp. 1225–1233, 2007.

[19] MTD Micromolding. *The 6 Sciences of Medical Micro Molding: How to Achieve Better Long-Term Results and Faster Speed to Market*. Accessed: Jul. 14, 2021. [Online]. Available: https://directory.qmed.com/p-free-white-paper-on-the-6-sciences-of-medical-file068602.html

[20] PTI Engineered Plastics. *The Benefits of Injection Molded Plastics in an EV/AV World*. Accessed: Jul. 14, 2021. [Online]. Available: https://directory.qmed.com/over-the-years-plastic-has-developed-into-one-of-file117915.html

[21] S. Olivera, H. B. Muralidhara, K. Venkatesh, K. Gopalakrishna, and C. S. Vivek, "Plating on acrylonitrile-butadiene-styrene (ABS) plastic: A review," *J. Mater. Sci.*, vol. 51, no. 8, pp. 3657–3674, 2016.

[22] Xometry. *The Ultimate Guide to Injection Molding*. Accessed: Jul. 14, 2021. [Online]. Available: https://www.xometry.com/ultimate-guide/injection-molding

[23] P. Leisner, M. Fredenberg, and I. Belov, "Pulse and pulse reverse plating of copper from acid sulphate solutions," *Trans. IMF*, vol. 88, no. 5, pp. 243–247, Sep. 2010.

[24] P. Adhikari, W. Yang, and D. Peroulis, "A 20–26.5-GHz PCB bandpass filter tuned with contactless tuners," *IEEE Microw. Wireless Compon. Lett.*, vol. 29, no. 8, pp. 513–515, Aug. 2019.

[25] J.-S. Hong, *Microstrip Filters for RF/Microwave Applications*, 2nd ed. Hoboken, NJ, USA: Wiley, 2011.

[26] R. J. Cameron, C. M. Kudsia, and R. R. Mansour, *Microwave Filters for Communication Systems: Fundamentals, Design, and Applications*, 2nd ed. Hoboken, NJ, USA: Wiley, 2018.

[27] D. M. Pozar, *Microwave Engineering*, 4th ed. Hoboken, NJ, USA: Wiley, 2012.

[28] P. Blondy and D. Peroulis, "Handling RF power: The latest advances in RF-MEMS tunable filters," *IEEE Microw. Mag.*, vol. 14, no. 1, pp. 24–38, Jan./Feb. 2013.

[29] K. Chen, A. Semnani, and D. Peroulis, "High-power microwave gas discharge in high-Q evanescent-mode cavity resonators and its instantaneous/long-term effects," in *IEEE MTT-S Int. Microw. Symp. Dig.*, Jun. 2013, pp. 1–4.

[30] A. Semnani, K. Chen, and D. Peroulis, "Microwave gas breakdown in tunable evanescent-mode cavity resonators," *IEEE Microw. Wireless Compon. Lett.*, vol. 24, no. 5, pp. 351–353, May 2014.

[31] S. Sirici, M. A. Sanchez-Soriano, J. D. Martinez, V. E. Boria, F. Gentili, W. Bosch, and R. Sorrentino, "Design and multiphysics analysis of direct and cross-coupled SIW combline filters using electric and magnetic couplings," *IEEE Trans. Microw. Theory Techn.*, vol. 63, no. 12, pp. 4341–4354, Dec. 2015.

[32] S. Saeedi, J. Lee, and H. Sigmarsson, "Prediction of power handling in tunable, high-Q, substrate-integrated, evanescent-mode cavity bandpass filters," *Electron. Lett.*, vol. 52, no. 10, pp. 846–848, May 2016.

[33] K. Sadasivan and D. Psychogiou, "Tunable 3D-printed coaxial-cavity filters with mixed electromagnetic coupling," in *Proc. IEEE Int. Symp. Antennas Propag. USNC-URSI Radio Sci. Meeting*, Jul. 2019, pp. 1703–1704.

[34] D. Psychogiou and K. Sadasivan, "Tunable coaxial cavity resonator-based filters using actuated liquid metal posts," *IEEE Microw. Wireless Compon. Lett.*, vol. 29, no. 12, pp. 763–766, Dec. 2019.

[35] F. Cai, W. Khan, and J. Papapolymerou, "A low loss X-band filter using 3-D polyjet technology," in *IEEE MTT-S Int. Microw. Symp. Dig.*, May 2015, pp. 8–11.
[36] S. Moon, H. H. Sigmarsson, H. Joshi, and W. Chappell, "Substrate integrated evanescent-mode cavity filter with a 3.5 to 1 tuning ratio," *IEEE Microw. Wireless Compon. Lett.*, vol. 20, no. 8, pp. 450–452, Aug. 2010.
[37] C. Ernst, V. Postoyalko, and N. G. Khan, "Relationship between group delay and stored energy in microwave filters," *IEEE Trans. Microw. Theory Techn.*, vol. 49, no. 1, pp. 192–196, Jan. 2001.

MICHAEL D. SINANIS (Student Member, IEEE) received the B.Sc. degree in mechanical engineering from the Piraeus University of Applied Sciences, Athens, Greece, in 2001, and the M.B.A. and M.A. degrees from the University of Indianapolis, Indianapolis, IN, USA, in 2006 and 2010, respectively. He is currently pursuing the Ph.D. degree in industrial engineering with Purdue University, West Lafayette, IN, USA, focusing on low-cost, high-performance reconfigurable R.F. devices.

Since 2011, he has been a Staff Research Engineer with the ARES Group, Elmor Family School of Electrical and Computer Engineering, Purdue University, under Prof. D. Peroulis. He has extensive experience in microsystems and nanosystems manufacturing. He received numerous prestigious awards, including the College of Engineering Staff Award of Excellence, in 2014.

PINTU ADHIKARI (Member, IEEE) received the B.Sc. degree in applied physics, electronics, and communication engineering from the University of Dhaka, Dhaka, Bangladesh, in 2013, the M.Sc. degree in electrical and computer engineering from Marquette University, Milwaukee, WI, USA, in 2016, and the Ph.D. degree in electrical and computer engineering from Purdue University, West Lafayette, IN, USA, in 2021. His research focuses on designing and manufacturing reconfigurable and automatically tunable microwave and millimeter-wave cavity tunable filters. He is a member of the IEEE Microwave Theory and Techniques Society (IEEE MTT-S). He received the Third Place Award of the Student Design Competition on Reconfigurable Microwave Filters of the IEEE MTT-S, IMS 2018.

THOMAS R. JONES (Member, IEEE) received the B.Sc. and Ph.D. degrees in electrical and computer engineering from the University of Alberta, in 2007 and 2019, respectively.

From 2008 to 2013, he worked in industry as a Project Engineer at Tracer Industries Canada Ltd. In 2013, he joined the Microwave to Millimeter-Wave (M2M) Group, University of Alberta, as a Research Assistant, where he is currently a Postdoctoral Fellow. He is also a Visiting Postdoctoral Fellow at Purdue University. His research interests include microwave and millimeter-wave design for wireless and satellite communication systems, reconfigurable RF front ends and tunable filters, and the microfabrication of on-chip millimeter-wave devices.

Dr. Jones was a recipient of the Queen Elizabeth II Graduate Scholarship, the Alberta Innovates Technology Futures (AITF) Graduate Student Scholarship, the Natural Science and Engineering Research Council (NSERC) Alexander Graham Bell Canada Graduate Scholarship, and the NSERC Postdoctoral Fellowship. He was also a recipient of the First Place Excellence in Nanofabrication Award at the 2017 CMC TEXPO Student Design Competition held in Montreal. He has served as the Finance Chair for the IEEE 2019 Canadian Conference on Electrical and Computer Engineering, and currently serves as the Vice-Chair for the Award-Winning IEEE Northern Canada Section AP-S/MTT-S Joint Chapter.

MAHMOUD ABDELFATTAH (Member, IEEE) received the B.S. degree in electrical engineering from Princess Sumaya University for Technology, Amman, Jordan, in 2014, and the Ph.D. degree in electrical and computer engineering from Purdue University, West Lafayette, IN, USA, in 2019.

He is currently a RF/EM Design Engineer with Skyworks Solutions Inc., Newbury Park, CA, USA. His current research interests include the design of multi-chip modules for handset RF front-end applications, manufacturing and control of reconfigurable microwave and millimeter wave cavity filters, lumped-element and planar filters, and microwave and millimeter-wave passive components.

Mr. Abdelfattah is a member of the IEEE Microwave Theory and Techniques Society (IEEE MTT-S). He was a recipient of the IEEE WAMICON Best Paper in Conference Award, in 2018, and the Second Place Award of the Student Design Competition on Switchable RF-MEMS Filter in the IEEE MTT-S IMS 2016.

DIMITRIOS PEROULIS (Fellow, IEEE) received the Ph.D. degree in electrical engineering from the University of Michigan at Ann Arbor, Ann Arbor, MI, USA, in 2003.

He is currently the Reilly Professor and the Michael and Katherine Birck Head of the Elmore Family School of Electrical and Computer Engineering, Purdue University, West Lafayette, IN, USA. He also serves as a Special Adviser for the Dean of Engineering on online learning. He has contributed to developing high-quality, widely tunable filters and novel filter architectures based on miniaturized high-Q cavity-based resonators in the 1–100-GHz range. He is also leading research efforts in high-power multifunctional RF electronics based on cold-plasma technologies. He has coauthored over 380 journal articles and conference papers. His research interests are focused on the areas of reconfigurable systems, cold-plasma RF electronics, and wireless sensors.

Dr. Peroulis received the National Science Foundation CAREER Award in 2008, the Outstanding Young Engineer Award, and the "Tatsuo Itoh" Award from the IEEE Microwave Theory and Techniques Society (MTT-S) in 2014 and 2019, respectively, the Outstanding Paper Award from the IEEE Ultrasonics, Ferroelectrics, and Frequency Control Society (Ferroelectrics Section) in 2012, and ten teaching awards, including the 2010 HKN C. Holmes MacDonald Outstanding Teaching Award, and the 2010 Charles B. Murphy Award, which is Purdue University's highest undergraduate teaching honor. His students have received numerous student paper awards and other student research-based scholarships. He has been a Purdue University Faculty Scholar.